

SONIC: Spectral Optimization of Noise for Inpainting with Consistency

Seungyeon Baek¹ Erqun Dong¹ Shadan Namazifard¹ Mark J. Matthews^{2,*} Kwang Moo Yi¹
¹ University of British Columbia ² Google DeepMind

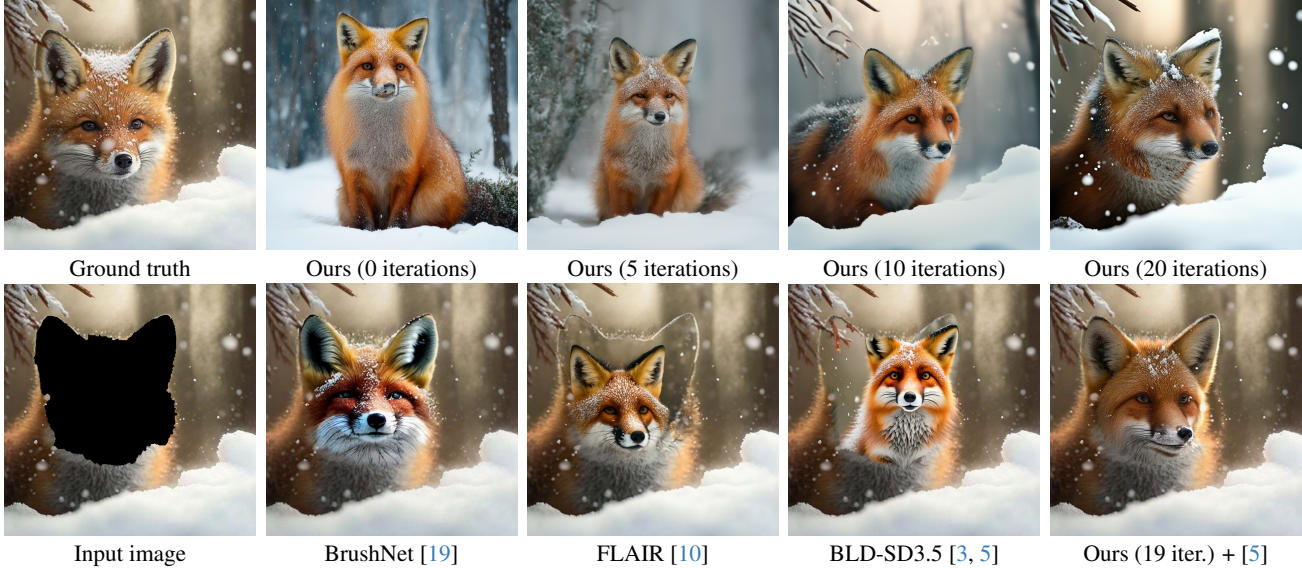


Figure 1. **Teaser** – We propose a novel training-free method of inpainting that focuses exclusively on the initial seed noise. (**Top row**) We show the denoising result of an initial seed noise, as we optimize the seed noise using our method. We optimize the seed noise to faithfully regenerate the non-masked regions of the input image, so as to obtain more consistent inpainting results. (**Bottom row**) Inpainting results of competing methods, with our final result on the right.

Abstract

We propose a novel training-free method for inpainting with off-the-shelf text-to-image models. While guidance-based methods in theory allow generic models to be used for inverse problems such as inpainting, in practice, their effectiveness is limited, leading to the necessity of specialized inpainting-specific models. In this work, we argue that the missing ingredient for training-free inpainting is the optimization (guidance) of the initial seed noise. We propose to optimize the initial seed noise to approximately match the unmasked parts of the data—with as few as a few tens of optimization steps. We then apply conventional training-free inpainting methods on top of our optimized initial seed noise. Critically, we propose two core ideas to effectively implement this idea: (i) to avoid the costly unrolling required to relate the initial noise and the gener-

ated outcome, we perform linear approximation; and (ii) to stabilize the optimization, we optimize the initial seed noise in the spectral domain. We demonstrate the effectiveness of our method on various inpainting tasks, outperforming the state of the art. Project page: <https://ubc-vision.github.io/sonic/>

1. Introduction

Denoising diffusion models [16, 40] and more recently flow models [26, 28] have become the go-to solution for various inverse problems in Computer Vision [9]. For example, most modern image inpainters [5, 17] utilize them in one way or another, including those that use pre-trained models with guidance [5, 27, 32], and those that train a conditional inpainting specific model [19, 57]. Diffusion and flow methods have also been used for inverse problems in other domains, such as image super-resolution and deblur-

*Participated in an advisory capacity only.

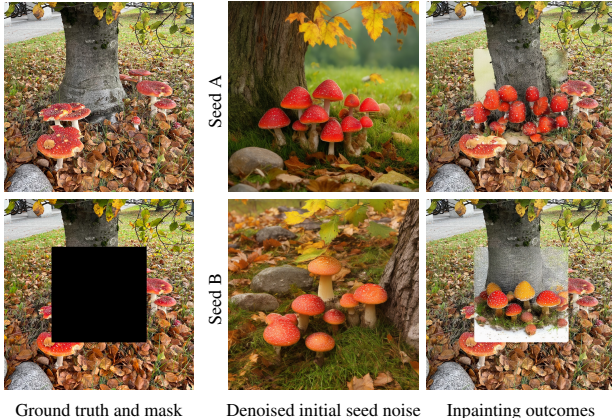


Figure 2. Initial seed noise already determines content – We show example inpainting outcomes of BLD [5] with StableDiffusion 3.5 backbone [3] using different initial seed noise. We show how different initial seeds denoise to different scene compositions even with the *same* prompt, and the final inpainting outcomes with each seed. Note how the content within the inpainted region, while modified, share similar structure as the denoised initial seed.

ring [10, 22, 32].

Among the many, we are similarly drawn to off-the-shelf models [5, 10, 22, 32] for inpainting, due to the versatility afforded by bypassing expensive training [19, 55] and task-specific augmentations that may not always generalize.¹ Unfortunately, the performance of existing training-free methods [5, 10, 22, 32] are not as good as their more specialized counterparts [19]; see Fig. 1.

In this work, we argue that the shortcomings of existing training-free methods, which rely on posterior sampling [10, 22] or conditioning [5, 32], are due to an oversight—the initial seed noise. Recent works [25, 43] have demonstrated that, already at the initial denoising step, much of the structure of the final denoised outcome is decided. For inpainting however, this is largely ignored, with the exception of very recent works [10] that begin to incorporate the initial seed noise in their framework. We, however, go beyond simply incorporating, and focus *solely* on the initial random noise. As shown in Fig. 2, the initial seed noise has a profound impact on the structure of the final generation.

We thus propose to *optimize* the initial seed noise, such that, once denoised, the observed portions of the image (the unmasked parts) match the target image. We present two key contributions that make doing so possible.

Our first contribution is an optimization strategy that *linearizes* the entire denoising (flow) trajectory. A naive approach would be to back-propagate through the entire unrolled denoising process to the initial noise, which quickly

¹We show later in experiments that, *e.g.*, BrushNet [19] produces inpainting mask specific results in some cases.



Figure 3. Optimizing in the spectral domain is important – We show examples of how the optimized initial seed noise denoises during the optimization process, when optimized to match the non-masked regions in Fig. 2, for seed A. While optimizing in the spatial domain also guides towards desired scene composition, optimizing in the spectral domain provides much more stable and robust optimization.

becomes impractical due to memory and compute requirements. Instead, we approximate the entire denoising trajectory as a linear path, allowing us to optimize the initial seed noise *without back-propagating through the denoiser*.

Our second contribution is the critical observation that *optimizing the noise must be done in the spectral domain*. Various works on spectral and time-based guidance scaling have hinted at this [12, 37, 53]—that different frequencies in the latent space have different preferences for the rate of change. We account for this by optimizing the initial seed noise in the spectral domain, obtaining significantly stabler optimization and convergence; see Fig. 3.

Implementation of this idea, however, requires care. We find that a naive implementation can lead to corruption of the initial seed noise, moving it away from the manifold of acceptable initial seed noises. To prevent this, we mask out gradient updates to unobserved data points, *i.e.*, masked pixels. We further find that the robustness of our method allows it to operate purely in latent space with simple nearest-neighbor fills for the masked regions when encoding masked images to the latent space.

To demonstrate the effectiveness of our method, we evaluate our method on three standard inpainting datasets: FFHQ [20], DIV2K [1], and BrushBench [19], each with different types of masks. On all three datasets, we outperform the state of the art in SSIM [46] and LPIPS [56] perceptual metrics, and Fréchet Inception Distance (FID) [14]. Our method is also often preferable in human preference scores such as HPS v2 [47] in terms of aesthetics.

Contributions. To summarize, our core contributions are:

- we propose a novel training-free method for inpainting,

which optimizes the initial seed noise to match the unmasked parts of the data;

- we propose a linear approximation strategy that allows us to optimize the initial seed noise *without back-propagating through the denoiser*;
- we propose to optimize in the *spectral domain*, which allows robust optimization;
- our method outperforms the state of the art in various inpainting tasks; and
- we will release code to facilitate reproduction.

2. Related Work

While various methods have been proposed to inpaint images, recent works have focused on utilizing the powerful generative prior of diffusion models [23, 27, 31, 45, 48, 49, 51, 52, 54]. We provide a brief review of works that utilize diffusion models, both training-free (ones that utilize generic models) and those that are trained or fine-tuned for the task of inpainting. For a more comprehensive review, we refer the reader to [17]. We also review a recent work that focuses on the importance of the initial seed noise and its effect on the denoising process.

Training-free methods. One of the key benefits of denoising diffusion models [16, 40] is their ability to be ‘guided’ by additional conditioning information [6, 13, 15]. The robustness of diffusion models under different manipulations naturally enables their use for inpainting. Some methods [5, 29] *blend* the noise within the masked region with the unmasked ground-truth noised image to condition the generation process. Others extend the Markov chain settings to be conditional [21] or perform range-null space decomposition [44]. Some more recent methods aim to sample from the posterior [8, 10, 22, 32, 36], such that the observed data points can be treated as the likelihood while the generic diffusion model serves as the prior; others focus on manipulating the geometry of the sampling trajectory [39].

A notable recent method along these lines is FLAIR [10], which formulates a variational method for posterior sampling. Interestingly, in their work, the final algorithm involves keeping track of *both* the final reconstruction and the *initial noise*. While these models all have shown improved performance beyond the original latent blending work [29], they still suffer from the same problem—their inpainting results often have an image structure that is inconsistent with the target image;² see Fig. 2. We posit that the missing ingredient in these methods is a proper intervention on the initial seed noise.

Importance of initial seed noise. Recent works [2, 25, 30, 43] have revealed how much influence the initial noise has on the final generation. Li *et al.* [25], demonstrate that the

initial seed largely determines the general layout of the generated image, and mine seeds that are more likely to produce better generations. Similarly, Ahn *et al.* [2], train a neural network to modify the initial seed noise to generate those that lead to better generations. Lyu *et al.* [30] generate a semantically meaningful initial seed with an automatic refinement pipeline. Very recently, an in-depth study [43] using Principal Component Analysis (PCA), revealed that the initial noise can reliably predict the image layout. All of these works hint at the same thing—that the initial seed noise must be considered if we are to match the structure of the image during inpainting.

Trained methods. Various methods have been proposed that *train* or *fine-tune* existing models. Effectively, these models circumvent the initial noise problem by training inpainting models that ignore the structure imposed by the initial seed noise. Common strategies include providing an inpainting mask and the encoded masked images as additional input and finetuning a pretrained model [34] with randomly masked images [41]. These can include having inpainting as a part of a multi-task adaptation via finetuning and prompt learning [57]. Some separate masked-image features and noisy latents to make the task easier to learn [19], some utilize semantics [7], and others train inpainting adapters [8, 48]. These methods, however, require additional training which can be costly, and as we show empirically later in Sec. 4, can fail to generalize to mask types not seen during training.

Concurrent work. Very recently, a *concurrent* work [35] of similar spirit, also proposes optimizing the initial seed noise for image editing based on image inversion. In their work, instead of linearizing as we do, they simply drop the Jacobian from the update rule, which leads to a similar equation as ours. Their optimization is done in the spatial domain, which we show empirically in Sec. 4.3 produces inferior results. This may be why their method utilizes an initial inversion step [18]; such initialization is not straightforward for inpainting tasks where some parts of the image are missing.

3. Method

3.1. Overview

An overview of our method is provided in Fig. 4. Our method focuses solely on finding the initial seed noise that best fits a partial (masked) observation. Our key innovation is a linearization strategy that allows optimization of the initial noise *without back-propagating through the denoiser*. We first formalize the problem, then explain our linear approximation and optimization strategy. We then introduce our spectral optimization, as well as subtle but important implementation details.

²FLAIR [10] suffers less from this, as they also directly manipulate the initial noise, but as we show later in Sec. 4 the effect is still present.

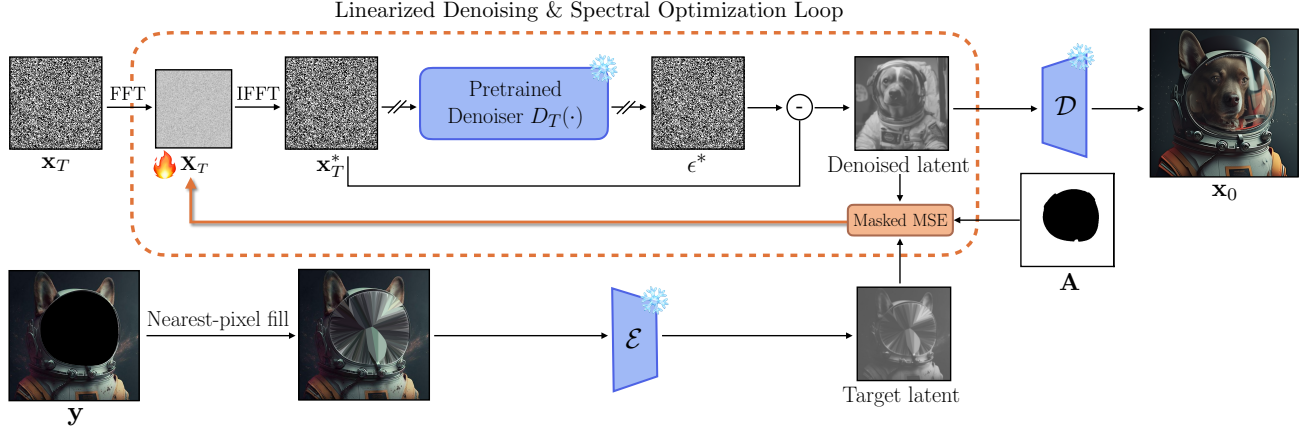


Figure 4. **Method overview** – We optimize the initial seed noise in the spectral domain \mathbf{X}_T , starting from a random noise \mathbf{x}_T , such that our denoised latent matches the masked observation \mathbf{y} in the latent space. To allow partial observations to be encoded, we use nearest-pixel filling before passing it into the encoder. We then compute the masked mean square error in the latent space, comparing it with a *fully denoised* latent and update \mathbf{X}_T accordingly. Importantly, we linearize the entire T step denoising process, essentially disconnecting the gradient flow passing through it. This allows us to optimize the initial seed noise \mathbf{X}_T *without back-propagating through the denoiser*.

Formalization. More formally, let \mathbf{y} be a corrupted (masked) image and \mathbf{A} be the corruption operator (mask), often denoted as a matrix in a slight abuse of notation. Let \mathbf{x}_T be the initial noise of a T -step denoising process, such that we can write the denoising process as $\mathbf{x}_0 = \mathcal{D}_T(\mathbf{x}_T)$, where \mathcal{D}_T is the T -step denoiser (e.g., a flow model [11]) and \mathbf{x}_0 is the fully denoised image. We aim to find the initial noise \mathbf{x}_T^* such that, when denoised $\mathcal{D}_T(\mathbf{x}_T^*)$, then corrupted, it matches the observed image \mathbf{y} . We formulate this as an optimization problem in a least-squares sense:

$$\mathbf{x}_T^* = \arg \min_{\mathbf{x}_T} \|\mathbf{y} - \mathbf{A} \mathcal{D}_T(\mathbf{x}_T)\|_2^2. \quad (1)$$

In this work, we focus on inpainting, thus \mathbf{A} is simply a binary mask. Note that, contrary to other methods, we do not alter the denoising process itself, but *only the initial noise* \mathbf{x}_T . While a noise that exactly satisfies $\mathbf{y} = \mathbf{A} \mathcal{D}_T(\mathbf{x}_T^*)$ may not exist, our method still provides an *enhanced* starting point for *any* denoising process.

Naively optimizing \mathbf{x}_T would mean back-propagating through $\mathcal{D}_T(\cdot)$, an expensive iterative process requiring unrolling the entire sequence, costly both in memory and compute—in fact, with an NVidia RTX 5090, back-propagating through more than one denoising step for Stable Diffusion 3.5 [3] is not feasible. We thus propose a linear approximation to circumvent this issue.

3.2. Optimizing without heavy back-propagation

We take advantage of the fact that denoising trajectories, especially for modern flow models [26, 28], are approximately linear.

Denoising trajectory linearization. We approximate the

denoising trajectory $\mathbf{x}(t)$, with a linear equation of the form:

$$\mathbf{x}(t) \approx \hat{\mathbf{x}}(t) = [\mathcal{D}_T(\mathbf{x}_T) - \mathbf{x}_T]_{\text{sg}} \left(1 - \frac{t}{T}\right) + \mathbf{x}_T, \quad (2)$$

where $t \in [0, T]$ and $[\cdot]_{\text{sg}}$ is the stop-gradient operator, implying that we consider the term $\mathcal{D}_T(\mathbf{x}_T) - \mathbf{x}_T$ to be constant throughout the denoising process. While in theory this should be a perfect approximation of flow models [26, 28], as they assume a straight trajectory, in practice the approximation error still exists. We find, however, that even with this linear assumption, we can still stably converge to an initial seed noise that generates observed images (Fig. 3) when combined with our spectral optimization (Sec. 3.3).

Optimization objective in the spatial domain. Given our linearization, we can now replace $\mathcal{D}_T(\mathbf{x}_T)$ in Eq. (1) with $\hat{\mathbf{x}}(0)$ from Eq. (2), and formulate a loss that optimizes for \mathbf{x}_T^* :

$$\mathcal{L}_{\text{linear}} = \left\| \mathbf{y} - \mathbf{A} \left([\mathcal{D}_T(\mathbf{x}_T) - \mathbf{x}_T]_{\text{sg}} + \mathbf{x}_T \right) \right\|_2^2. \quad (3)$$

Note that Eq. (3) is differentiable with respect to \mathbf{x}_T , *without* any need for back-propagating through $\mathcal{D}_T(\cdot)$.

3.3. Optimizing in the spectral domain

In practice, when directly optimizing for \mathbf{x}_T^* via Eq. (3) we observe what appear to be regional instabilities in the *spectra* of \mathbf{x}_T —denoised image flickering between optimization steps, showing different levels of detail, *i.e.*, *spatial frequencies* converging in different pace. This observation, combined with recent works that treat different frequencies of the latent space differently during guidance [12, 37, 53],

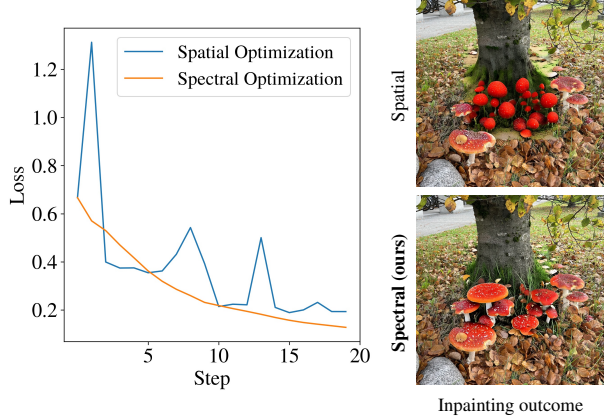


Figure 5. Optimizing in the spectral domain – (Left) We show an example convergence graph of Eq. (3) when optimizing in the spatial domain vs spectral, for the same example in Fig. 3. **(Right)** We show the final inpainting outcomes for both domains. Optimizing in the spectral domain provides a seamless inpainting outcome, whereas in the spatial domain it fails.

motivate us to instead optimize in the *spectral* domain, so as to *level* the learning pace with respect to frequency. Instead of treating \mathbf{x}_T as a trainable parameter, we optimize its spectral representation \mathbf{X}_T , defined as the Fourier transform of \mathbf{x}_T , *i.e.*, $\mathbf{x}_T = \mathcal{F}^{-1}(\mathbf{X}_T)$. We observe stabler convergence behavior when optimizing \mathbf{X}_T (see Fig. 5), while optimizing \mathbf{x}_T tends to produce initial seed noise outside the typical initial noise manifold, causing over-saturation and degradation in image quality (as previously seen in Fig. 3). While this technically is a small change, it has a significant impact on the quality of the inpainting outcomes—to a degree where spatial optimization often results in inpainting failures. We further ablate this choice in Sec. 4.3.

3.4. Implementation details

With our method presented, we now discuss subtle yet important implementation details that are critical for the method to work.

Masking out gradient updates. A critical component to consider is that, our optimized initial seed noise must remain within the manifold of acceptable initial seed noises. A naive implementation of our idea, even with spectral optimization, can still lead to corruption because of gradient updates that ‘seep’ into the unobserved data points, *i.e.*, masked pixels. As shown in Fig. 6, if untreated, these updates cause the initial seed noise within the masked region to ‘drift away’ causing visible artifacts such as darkening, saturation, or frame-level artifacts. To prevent this, we mask out gradient updates to the unobserved data points, *i.e.*, the masked region of the latent, and preserve the ideal Gaussian-sampled distribution.

Masking in the latent space. Another computational bot-

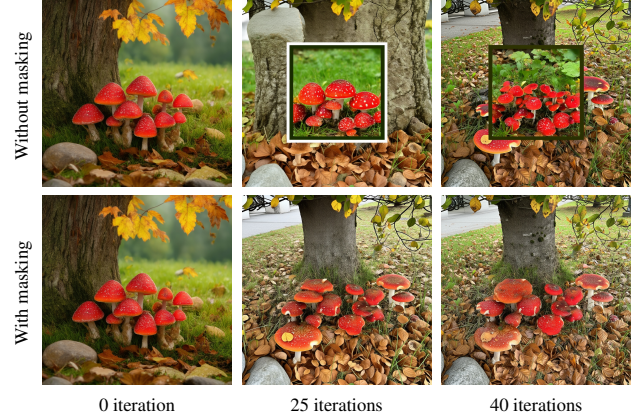


Figure 6. Masking out gradient updates is important – We show how the initial seed noise denoises, similarly to Fig. 3, but with and without masking out updates within the unobserved (masked) region. As shown, without masking, the optimization diverges from the initial seed manifold, causing the visible colour shifts, artifacts and mask borders as optimization progresses.

tleneck, aside from back-propagation through the denoiser or the flow estimation, is the Variational Auto-Encoder (VAE) that maps images to the latent space. Thanks to the robustness of our method, we find that we can safely perform all operations in the latent space, by simply filling in the masked region pixels with their nearest-neighbor colors; see Fig. 4. While this does not look like a proper inpainted image, we empirically find that this is sufficient. We compare this simple fill-in strategy against the *upper-bound* performance of directly using the ground-truth image in Sec. 4.3.

Other details. We implement our method with StableDiffusion 3.5 [3], and with BLD-SD3.5 [3, 5] as the inpainter starting from our optimized initial seed noise. To optimize the initial seed noise, we use the Adam [24] optimizer with learning rate of 3.0, and with default parameters $\beta_1 = 0.9$ and $\beta_2 = 0.999$. We use a classifier-free guidance [15] scale of 2.0, following FLAIR [10]. We set the image resolution as 1024×1024 for all our experiments to match the expected input size of SD 3.5. We also use $T = 20$ for our denoiser.

4. Results

We first discuss our experimental setup, then present our results, and finally ablate our design choices.

4.1. Experimental setup

Datasets and masks. We evaluate our method on three standard datasets, using different types of masks on each.

- **FFHQ [20]:** A standard dataset often used for evaluating image inpainting methods, containing 70,000 high-

quality face photographs with diverse age, pose, and accessories. We follow the protocol in FLAIR [10], using the first 1000 images and applying a large, rectangular mask with a fixed size and position that covers approximately half of the subject’s face.

- **DIV2K [1]**: A set of 1,000 2K high-resolution natural images. Again, we follow the protocol of FLAIR [10] by taking 800 images from the training set. Then, we apply the same masking pattern to all samples, consisting of six randomly positioned rectangular regions.³
- **BrushBench [19]**: 600 natural and artificial images with human-annotated masks based on segmentation, and captions. We use the provided inpaint segmentation masks and prompts.

Prompts. As diffusion/flow-based inpainting methods require prompts, we systematically generate prompts through a Vision Language Model (VLM) [4] For FFHQ [20] and DIV2K [1]. We provide the masked images and prompt the VLM to infer the contents of the image and describe them in two to three concise sentences. The exact prompt used for the VLM can be found in Supplementary Material. We use the generated prompts for *all* methods, including ours. For BrushBench [19] we simply use the standard dataset-provided prompts.

Baselines. We compare our method against the following baselines:

- **BLD-SD3.5 [3, 5]**: Adopted by diffusers [42] as the default inpainting pipeline, it is a training-free method that ‘blends’ the denoising process in the masked region with the ground-truth denoising trajectory of the unmasked region.
- **FlowChef [32]**: Improves trajectories and stability for flow/diffusion models when solving inverse problems.
- **FlowDPS [22]**: A flow-based posterior sampling method for inverse problems with explicit guidance. Following FLAIR [10], we implement an inpainting solver for this method.
- **FLAIR [10]**: A recent training-free inverse problem solver that uses a variational formula involving update of both initial noise and final estimates.
- **BrushNet [19]**: A trained method that specializes in inpainting. We use the Stable Diffusion 1.5 [34] checkpoint from the official implementation, and their standard classifier-free guidance scale of 7.5. BrushNet offers two model subtypes: one trained with random masks, and another with segmentation masks. We use the former for FFHQ [20] and DIV2K [1] while using the latter for BrushBench [19].

For fairness, following FLAIR [10], we use the *same* StableDiffusion 3.5 [3] (‘medium’ variant) base model for training-free methods (BLD-SD3.5 [3, 5], FlowChef [32],

³We use the exact same locations as FLAIR [10].

FlowDPS [22], FLAIR [10], and ours). We set the classifier-free guidance scale to 2.0 for these methods, as in FLAIR [10]. Additionally, as the baselines generate varying resolution outputs, we process the images at their native resolution (varying from 512×512 to 768×768) and resize to 1024×1024 for evaluation.

For each baseline, we report performance at their suggested number of function evaluations (NFE) and at 400 NFE, which we use for our method. Note, however, that as our method does not back-propagate through the denoiser, our runtime is comparable to methods with a lower NFE—taking approximately a minute to inpaint one image on a GeForce RTX 5090 GPU, roughly the same time as FLAIR [10] using 50 NFE.

Evaluation metrics. To quantify the quality of the inpainting results, we use the standard metrics: Peak Signal-to-Noise Ratio (PSNR), Structural Similarity Index Measure (SSIM) [46], Learned Perceptual Image Patch Similarity (LPIPS) [56], Fréchet Inception Distance (FID) [14], as well as CLIP score (Contrastive Language–Image Pre-training) [33]. We also use metrics that are designed to mimic human preference: Image Reward (IR) [50], Human Preference Score v2 (HPS v2) [47], and Aesthetic Score (AS) [38].

For the task of inpainting, where many different answers can exist, we warn that PSNR should be considered with care—*lower PSNR does not necessarily mean worse performance*, as also discussed in [10]. Instead, all metrics should be considered altogether. Still, if a few metrics were to be weighed strongly, we argue that LPIPS and FID are the *most important* for evaluating inpainting quality as they evaluate how similar the inpainted content is to the ground truth via ‘perceived’ similarity. This tolerates minor differences in exact structure and color, which are acceptable in the context of inpainting. CLIP score gauges how well the inpainting results match the original content *semantically*, but should also be read carefully, as the inpainted content may be *geometrically* misaligned with the image. IR, HPS v2, AS are also imperfect metrics, as they are designed to measure image quality, not inpainting quality.

4.2. Results

We present qualitative results in Fig. 7. We compare our method against FLAIR [10], BrushNet [19], and BLD-SD3.5 [3, 5]. We provide additional qualitative results in the Supplementary Material. We also provide per-dataset quantitative summaries in Tabs. 1 to 3.

FFHQ [20] – Fig. 7 and Tab. 1. As seen in Fig. 7, our method significantly outperforms other baselines, followed by FLAIR [10]. BrushNet [19] is great at hiding seams, as it is a trained method, but the content it inpaints can misalign with the full image. In the case of BLD-SD3.5 [3, 5], it

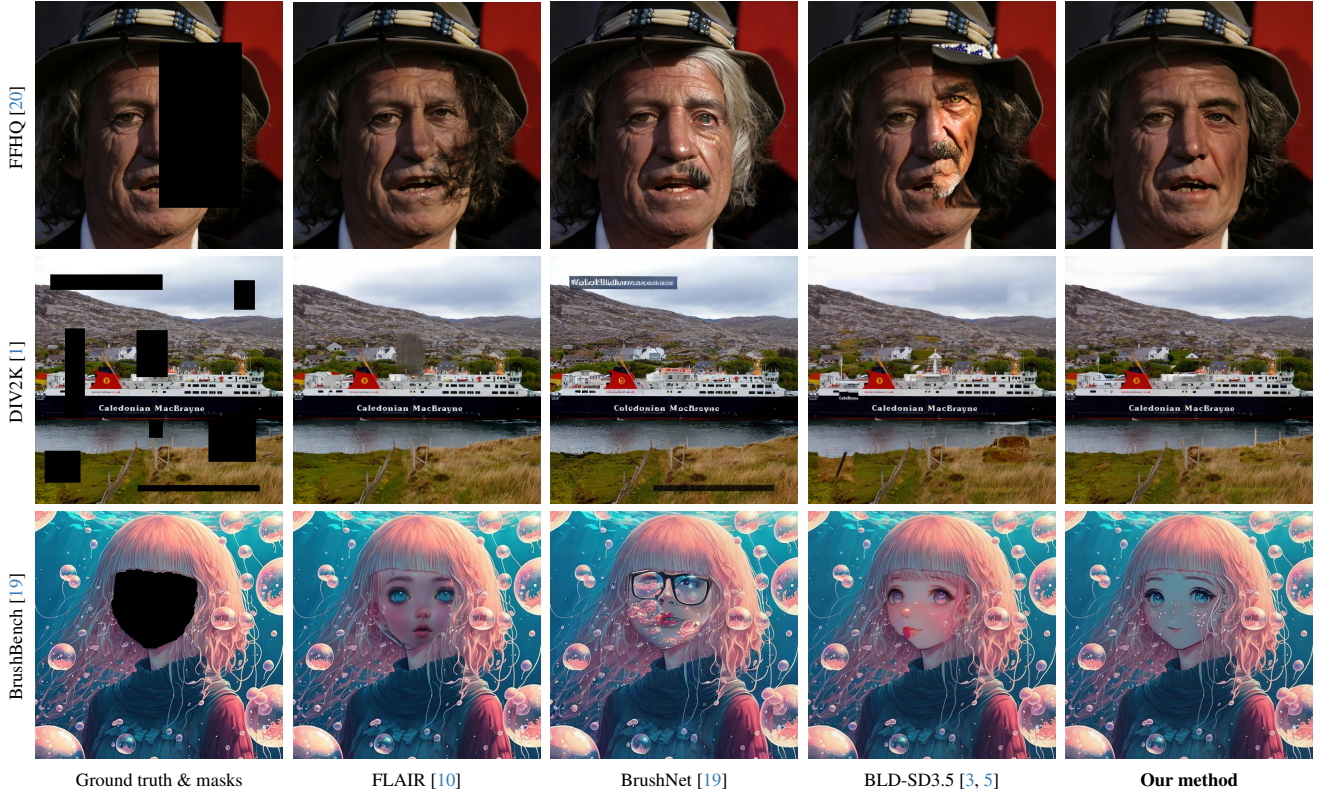


Figure 7. **Qualitative results** – We show results across different methods and datasets. We denote the masked areas with black rectangles on the ground truth images. Our method provides the best inpainting results, especially aligning well with the layout and also the lighting conditions of the input image. Zoom in for better detail.

Table 1. **Quantitative results on FFHQ [20]** – Our method outperforms all other methods in terms of SSIM, LPIPS, and FID by a large margin. Our method also performs best in terms of simulated human preference metrics, IR and HPS v2, and second best in AS. Note that while PSNR is lower, this does not mean our method provides worse results, as for inpainting, an image different from ground-truth may still be correct. FlowDPS [22] performs best in terms of CLIP scores, but notice the significantly higher LPIPS and FID scores, indicating poor inpainting quality.

| Method | PSNR↑ | SSIM↑ | LPIPS↓ | FID ↓ | IR ↑ | HPS v2↑ | CLIP↑ | AS↑ |
|--------------------------|---------------|--------------|--------------|----------------------------|--------------|---------------|--------------|-----|
| BrushNet [19] | 21.929 | 0.759 | 0.237 | 17.950 0.100 | 0.229 | 20.983 | 5.713 | |
| BLD-SD3.5 [3, 5] | 17.592 | 0.824 | 0.180 | 25.842 -0.277 | 0.206 | 19.099 | 5.136 | |
| FLAIR [10] | 23.100 | 0.823 | 0.266 | 18.982 0.088 | 0.228 | 20.632 | 5.735 | |
| FLAIR [10] (400 NFEs) | 24.099 | 0.829 | 0.292 | 19.873 0.069 | 0.225 | 20.439 | 5.537 | |
| FlowChef [32] | 19.624 | 0.828 | 0.193 | 20.706 -0.189 | 0.207 | 19.342 | 5.075 | |
| FlowChef [32] (400 NFEs) | 19.336 | 0.824 | 0.197 | 21.191 -0.198 | 0.206 | 19.227 | 5.029 | |
| FlowDPS [22] | 20.215 | 0.760 | 0.374 | 48.333 -0.112 | 0.225 | 22.360 | 5.793 | |
| FlowDPS [22] (400 NFEs) | 23.243 | 0.786 | 0.389 | 68.644 -0.065 | 0.223 | 22.420 | 5.926 | |
| Our method | 22.562 | 0.857 | 0.121 | 12.883 0.114 | 0.233 | 20.773 | 5.849 | |

completely fails to align the global structure, resulting in an inpainting failure. These findings are also reflected in the quantitative metrics presented in Tab. 1, with our method outperforming all other methods in terms of SSIM, LPIPS, FID, IR, and HPS v2. In terms of FID, our method out-

performs all other methods by a large margin, with BrushNet [19] being the second best and FLAIR [10] being the third best. As BrushNet [19] does not have seams, it shows up favorably in FID, and other aesthetic metrics. But in terms of SSIM and LPIPS, where structure is considered, the method performs significantly worse. While we perform worse in terms of PSNR and CLIP score, we emphasize again that these in isolation *do not* directly correlate with inpainting performance.

DIV2K [1] – Fig. 7 and Tab. 2. Our method performs best for this dataset as well. FLAIR [10] struggles and produces blurry patches, which may be why it shows high PSNR in Tab. 2, but lower SSIM and LPIPS scores. BrushNet [19], in this example, produces caption-like inpainting results in horizontal stripe masks, hinting that its inpainting outcomes are strongly correlated with the shape of the mask. The quantitative results in Tab. 2 further show how this method significantly performs worse than other methods for this dataset. BLD-SD3.5 [3, 5] does not show apparent artifacts, but as can be seen in the square mask in the bottom right, or the vertical mask on the left, its inpainting results do not align well with the full image. Again, for this dataset, our method outperforms all other methods in terms of SSIM,

Table 2. **Quantitative results on DIV2K [1]** – Our method performs best in terms of SSIM, LPIPS, and FID by a large margin. We also perform best in terms of HPS v2. While FLAIR [10] shows high PSNR, as shown in Fig. 7, this could be attributed to the fact that it produces blurry patches. FLAIR [10] also has high IR and AS, and FlowChef [32] and BrushNet [19] show higher CLIP scores, but they all perform significantly worse in terms of LPIPS and FID, indicating poor inpainting quality.

| Method | PSNR↑ | SSIM↑ | LPIPS↓ | FID↓ | IR↑ | HPS v2↑ | CLIP↑ | AS↑ |
|--------------------------|---------------|--------------|--------------|---------------|--------------|--------------|---------------|--------------|
| BrushNet [19] | 19.414 | 0.575 | 0.308 | 29.004 | 0.295 | 0.244 | 24.197 | 5.406 |
| BLD-SD3.5 [3, 5] | 19.768 | 0.789 | 0.144 | 25.328 | 0.355 | 0.250 | 23.721 | 5.883 |
| FLAIR [10] | 23.128 | 0.760 | 0.298 | 22.421 | 0.364 | 0.246 | 23.839 | 5.909 |
| FLAIR [10] (400 NFEs) | 23.250 | 0.768 | 0.294 | 22.147 | 0.402 | 0.249 | 23.751 | 5.929 |
| FlowChef [32] | 20.067 | 0.748 | 0.237 | 30.481 | 0.192 | 0.239 | 24.284 | 5.062 |
| FlowChef [32] (400 NFEs) | 19.938 | 0.747 | 0.238 | 30.769 | 0.196 | 0.240 | 24.289 | 5.084 |
| FlowDPS [22] | 20.596 | 0.628 | 0.424 | 46.611 | 0.227 | 0.238 | 24.017 | 5.802 |
| FlowDPS [22] (400 NFEs) | 21.728 | 0.650 | 0.420 | 67.893 | 0.111 | 0.231 | 24.186 | 5.514 |
| Our method | 21.284 | 0.803 | 0.115 | 17.699 | 0.352 | 0.250 | 23.777 | 5.927 |

Table 3. **Quantitative results on BrushBench [19]** – Our method outperforms all baselines in terms of SSIM, LPIPS, and FID. For other metrics, ours performs third-best. Unsurprisingly, BrushNet [19] performs second best in terms of FID, and best in terms of IR, HPS v2, and AS, as this dataset was developed by BrushNet [19]. But in terms of LPIPS and FID, they are worse than ours, in line with Fig. 7. FLAIR [10] again shows high PSNR and SSIM, but performs worse in all other metrics.

| Method | PSNR↑ | SSIM↑ | LPIPS↓ | FID↓ | IR↑ | HPS v2↑ | CLIP↑ | AS↑ |
|--------------------------|---------------|--------------|--------------|---------------|--------------|--------------|---------------|--------------|
| BrushNet [19] | 18.668 | 0.740 | 0.199 | 50.082 | 1.246 | 0.271 | 26.551 | 6.366 |
| BLD-SD3.5 [3, 5] | 18.234 | 0.854 | 0.169 | 51.661 | 1.211 | 0.267 | 27.262 | 6.072 |
| FLAIR [10] | 19.986 | 0.855 | 0.201 | 51.644 | 1.007 | 0.255 | 26.655 | 5.978 |
| FLAIR [10] (400 NFEs) | 20.154 | 0.855 | 0.190 | 51.535 | 1.025 | 0.255 | 26.455 | 5.878 |
| FlowChef [32] | 18.711 | 0.856 | 0.161 | 53.568 | 0.975 | 0.253 | 26.680 | 5.826 |
| FlowChef [32] (400 NFEs) | 18.688 | 0.853 | 0.161 | 52.281 | 1.025 | 0.256 | 26.767 | 5.877 |
| FlowDPS [22] | 18.269 | 0.775 | 0.360 | 67.731 | 0.895 | 0.248 | 27.045 | 5.909 |
| FlowDPS [22] (400 NFEs) | 18.558 | 0.795 | 0.338 | 80.544 | 0.832 | 0.241 | 26.742 | 5.813 |
| Our Method | 19.014 | 0.861 | 0.153 | 48.072 | 1.188 | 0.263 | 26.890 | 6.061 |

LPIPS, FID, and HPS v2.

BrushBench [19] – Fig. 7 and Tab. 3. Again, our method performs best. FLAIR [10], for this dataset, is unable to match the global structure of the image well and often produces a disjoint inpainting outcome. BrushNet [19], which is the method developed for this dataset, provides results that seamlessly align with the local surroundings, but often misaligns the rough global structure. BLD-SD3.5 [3, 5], for this example, produces arguably the second best results, which aligns with the FID-based evaluation in Tab. 3. Our method, quantitatively, outperforms all methods in terms of SSIM, LPIPS, FID, and performs third-best in terms of other metrics. We emphasize again, that each metric alone does not paint a complete picture of the inpainting quality, and all metrics should be considered together. Among them, we believe LPIPS and FID *best* represents the performance of each method, as it compares the perceived similarity between the inpainting results and the ground truth, tolerating

Table 4. **Ablation study** – We report the evaluation metrics for FFHQ [20] dataset with variants of our method: using spatial optimization; removing masking of gradient updates; and using ground-truth image as input to the encoder, which shows the upper-bound performance of operating in the latent space. Both spectral optimization and gradient masking are critical. Using ground-truth image for the encoder shows similar performance as our simple nearest-neighbor fill-ins, showing that this simple strategy is sufficient.

| Variant | PSNR↑ | SSIM↑ | LPIPS↓ | FID↓ | IR↑ | HPS v2↑ | CLIP↑ | AS↑ |
|------------------------|---------------|--------------|--------------|---------------|--------------|--------------|---------------|--------------|
| Spatial Optimization | 22.120 | 0.853 | 0.127 | 14.579 | 0.062 | 0.229 | 20.438 | 5.760 |
| w/o gradient masking | 18.863 | 0.833 | 0.165 | 33.269 | -0.389 | 0.215 | 19.564 | 5.364 |
| Optimizing with the GT | 22.569 | 0.856 | 0.121 | 12.773 | 0.115 | 0.233 | 20.807 | 5.850 |
| Our method | 22.562 | 0.857 | 0.121 | 12.883 | 0.114 | 0.233 | 20.773 | 5.849 |

minor differences in exact structure and color.

4.3. Ablation study

We perform ablation studies to motivate our design choices. For the ablation study, we use the FFHQ [20] dataset. We summarize the quantitative results in Tab. 4. Observe that both optimizing in the spectral domain and masking out gradient updates is critical to the performance of the method. Additionally, optimizing with the nearest-neighbor fill-in produces similar metrics as optimizing with the ground truth image, which would be the upper-bound performance. This confirms the robustness of our method, and that the simple fill-in strategy is sufficient.

5. Conclusion

We presented a novel training-free method for inpainting that focuses on the initial seed noise. We have shown that by finding the right initial seed noise through optimization, we can achieve inpainting results that outperform the state of the art. The key ideas that enable this are the linear approximation strategy that allows optimization of the initial noise without back-propagating through the denoiser, and spectral domain optimization that ensures stable convergence. Masking gradient updates further ensures that the optimization does not stray from the initial seed noise manifold. We conduct experiments on three standard inpainting datasets FFHQ [20], DIV2K [1], and BrushBench [19], and demonstrate the effectiveness of our method.

Limitations and future work. While we have demonstrated our method purely within the inpainting task, the formulation behind the method, in theory, could be applied to other inverse problems such as super-resolution, deblurring, and video inpainting. We hope our work can serve as a starting point for future research on directly utilizing generic flow models for various inverse problems.

Acknowledgments. This work was supported in part by the Natural Sciences and Engineering Research Council of Canada (NSERC) Discovery Grant, NSERC Collaborative Research and Development Grant, NSERC Alliance Advantage Grant, Google, Digital Research Alliance of Canada, and Advanced Research Computing at the University of British Columbia.

References

- [1] Eirikur Agustsson and Radu Timofte. NTIRE 2017 challenge on single image super-resolution: Dataset and study. In *IEEE Conf. Comput. Vis. Pattern Recog. Worksh.*, 2017. [2](#), [6](#), [7](#), [8](#)
- [2] Donghoon Ahn, Jiwon Kang, Sanghyun Lee, Jaewon Min, Minjae Kim, Wooseok Jang, Hyoungwon Cho, Sayak Paul, SeonHwa Kim, Eunju Cha, Kyong Hwan Jin, and Seungryong Kim. A noise is worth diffusion guidance. *arXiv*, 2024. [3](#)
- [3] Stability AI. Stable diffusion 3.5 medium: A 2.5 billion parameter multimodal diffusion transformer. <https://huggingface.co/stabilityai/stable-diffusion-3.5-medium>, 2024. [1](#), [2](#), [4](#), [5](#), [6](#), [7](#), [8](#)
- [4] Anthropic. Claude code. <https://claude.com/claude-code>, 2025. [6](#), [12](#)
- [5] Omri Avrahami, Ohad Fried, and Dani Lischinski. Blended latent diffusion. *ACM Trans. Graph.*, 42(4), 2023. [1](#), [2](#), [3](#), [5](#), [6](#), [7](#), [8](#)
- [6] Arpit Bansal, Hong-Min Chu, Avi Schwarzschild, Soumyadip Sengupta, Micah Goldblum, Jonas Geiping, and Tom Goldstein. Universal guidance for diffusion models. In *Int. Conf. Learn. Represent.*, 2024. [3](#)
- [7] Yifu Chen, Jingwen Chen, Yingwei Pan, Yehao Li, Ting Yao, Zheneng Chen, and Tao Mei. Improving text-guided object inpainting with semantic pre-inpainting. In *Eur. Conf. Comput. Vis.*, 2024. [3](#)
- [8] Ciprian Corneanu, Raghudeep Gadde, and Aleix M. Martinez. Latentpaint: Image inpainting in latent space with diffusion models. In *IEEE Winter Conf. Appl. Comput. Vis.*, 2024. [3](#)
- [9] Giannis Daras, Hyungjin Chung, Chieh-Hsin Lai, Yuki Mitsufuji, Jong Chul Ye, Peyman Milanfar, Alexandros G. Dimakis, and Mauricio Delbracio. A survey on diffusion models for inverse problems. *arXiv*, 2024. [1](#)
- [10] Julius Erbach, Dominik Narnhofer, Andreas Dombos, Bernt Schiele, Jan Eric Lenssen, and Konrad Schindler. Solving inverse problems with flair. In *Adv. Neural Inform. Process. Syst.*, 2025. [1](#), [2](#), [3](#), [5](#), [6](#), [7](#), [8](#)
- [11] Patrick Esser, Sumith Kulal, Andreas Blattmann, Rahim Entezari, Jonas Müller, Harry Saini, Yam Levi, Dominik Lorenz, Axel Sauer, Frederic Boesel, Dustin Podell, Tim Dockhorn, Zion English, and Robin Rombach. Scaling rectified flow transformers for high-resolution image synthesis. In *International Conference on Machine Learning*, 2024. [4](#)
- [12] Zheng Gao, Jifei Song, ZhenSong Zhang, JianKang Deng, and Ioannis Patras. Frequency-guided diffusion for training-free text-driven image translation. In *Int. Conf. Comput. Vis.*, 2025. [2](#), [4](#)
- [13] Yutong He, Naoki Murata, Chieh-Hsin Lai, Yuhta Takida, Toshimitsu Uesaka, Dongjun Kim, Wei-Hsiang Liao, Yuki Mitsufuji, J. Zico Kolter, Ruslan Salakhutdinov, and Stefano Ermon. Manifold preserving guided diffusion. In *Int. Conf. Learn. Represent.*, 2024. [3](#)
- [14] Martin Heusel, Hubert Ramsauer, Thomas Unterthiner, Bernhard Nessler, and Sepp Hochreiter. Gans trained by a two time-scale update rule converge to a local nash equilibrium. In *Adv. Neural Inform. Process. Syst.*, 2017. [2](#), [6](#)
- [15] Jonathan Ho and Tim Salimans. Classifier-free diffusion guidance. In *NeurIPS 2021 Workshop on Deep Generative Models and Downstream Applications*, 2021. [3](#), [5](#)
- [16] Jonathan Ho, Ajay Jain, and Pieter Abbeel. Denoising diffusion probabilistic models. In *Adv. Neural Inform. Process. Syst.*, 2020. [1](#), [3](#)
- [17] Yi Huang, Jiancheng Huang, Yifan Liu, Mingfu Yan, Jiaxi Lv, Jianzhuang Liu, Wei Xiong, He Zhang, Liangliang Cao, and Shifeng Chen. Diffusion model-based image editing: A survey. *IEEE Trans. Pattern Anal. Mach. Intell.*, 47(6), 2025. [1](#), [3](#)
- [18] Guanlong Jiao, Binqing Huang, Kuan-Chieh Wang, and Renjie Liao. Unedit-flow: Unleashing inversion and editing in the era of flow models. *arXiv*, 2025. [3](#)
- [19] Xuan Ju, Xian Liu, Xintao Wang, Yuxuan Bian, Ying Shan, and Qiang Xu. Brushnet: A plug-and-play image inpainting model with decomposed dual-branch diffusion. In *Eur. Conf. Comput. Vis.*, 2024. [1](#), [2](#), [3](#), [6](#), [7](#), [8](#)
- [20] Tero Karras, Samuli Laine, and Timo Aila. A style-based generator architecture for generative adversarial networks. In *IEEE Conf. Comput. Vis. Pattern Recog.*, 2019. [2](#), [5](#), [6](#), [7](#), [8](#)
- [21] Bahjat Kawar, Michael Elad, Stefano Ermon, and Jiaming Song. Denoising diffusion restoration models. In *Adv. Neural Inform. Process. Syst.*, 2022. [3](#)
- [22] Jeongsol Kim, Bryan Sangwoo Kim, and Jong Chul Ye. Flowdps: Flow-driven posterior sampling for inverse problems. In *Int. Conf. Comput. Vis.*, 2025. [2](#), [3](#), [6](#), [7](#), [8](#)
- [23] Sora Kim, Sungho Suh, and Minsik Lee. Rad: Region-aware diffusion models for image inpainting. In *IEEE Conf. Comput. Vis. Pattern Recog.*, 2025. [3](#)
- [24] Diederik P. Kingma and Jimmy Ba. Adam: A method for stochastic optimization. In *Int. Conf. Learn. Represent.*, 2015. [5](#)
- [25] Shuangqi Li, Hieu Le, Jingyi Xu, and Mathieu Salzmann. Enhancing compositional text-to-image generation with reliable random seeds. In *Int. Conf. Learn. Represent.*, 2025. [2](#), [3](#)
- [26] Yaron Lipman, Ricky T. Q. Chen, Heli Ben-Hamu, Maximilian Nickel, and Matt Le. Flow matching for generative modeling. In *Int. Conf. Learn. Represent.*, 2023. [1](#), [4](#)
- [27] Kuan-Hung Liu, Cheng-Kun Yang, Min-Hung Chen, Yu-Lun Liu, and Yen-Yu Lin. Corrfill: Enhancing faithfulness in reference-based inpainting with correspondence guidance in diffusion models. In *IEEE Winter Conf. Appl. Comput. Vis.*, 2025. [1](#), [3](#)
- [28] Xingchao Liu, Chengyue Gong, and Qiang Liu. Flow straight and fast: Learning to generate and transfer data with rectified flow. In *Int. Conf. Learn. Represent.*, 2023. [1](#), [4](#)

[29] Andreas Lugmayr, Martin Danelljan, Andres Romero, Fisher Yu, Radu Timofte, and Luc Van Gool. Repaint: Inpainting using denoising diffusion probabilistic models. In *IEEE Conf. Comput. Vis. Pattern Recog.*, 2022. 3

[30] Yongzhe Lyu, Yu Wu, Yutian Lin, and Bo Du. Is-diff: Improving diffusion-based inpainting with better initial seed. *arXiv*, 2025. 3

[31] Hayk Manukyan, Andranik Sargsyan, Barsegh Atanyan, Zhangyang Wang, Shant Navasardyan, and Humphrey Shi. Hd-painter: High-resolution and prompt-faithful text-guided image inpainting with diffusion models. In *Int. Conf. Learn. Represent.*, 2025. 3

[32] Maitreya Patel, Song Wen, Dimitris N. Metaxas, and Yezhou Yang. Steering rectified flow models in the vector field for controlled image generation. In *Int. Conf. Comput. Vis.*, 2025. 1, 2, 3, 6, 7, 8

[33] Alec Radford, Jong Wook Kim, Chris Hallacy, Aditya Ramesh, Gabriel Goh, Sandhini Agarwal, Girish Sastry, Amanda Askell, Pamela Mishkin, Jack Clark, Gretchen Krueger, and Ilya Sutskever. Learning transferable visual models from natural language supervision. In *International Conference on Machine Learning*, 2021. 6

[34] Robin Rombach, Andreas Blattmann, Dominik Lorenz, Patrick Esser, and Björn Ommer. High-resolution image synthesis with latent diffusion models. In *IEEE Conf. Comput. Vis. Pattern Recog.*, 2022. 3, 6

[35] Or Ronai, Vladimir Kulikov, and Tomer Michaeli. Flowopt: Fast optimization through whole flow processes for training-free editing. *arXiv*, 2025. 3

[36] Litu Rout, Negin Raoof, Giannis Daras, Constantine Caramanis, Alexandros G. Dimakis, and Sanjay Shakkottai. Solving linear inverse problems provably via posterior sampling with latent diffusion models. In *Adv. Neural Inform. Process. Syst.*, 2023. 3

[37] Seyedmorteza Sadat, Tobias Vontobel, Farnood Salehi, and Romann M. Weber. Guidance in the frequency domain enables high-fidelity sampling at low cfg scales. *arXiv*, 2025. 2, 4

[38] Christoph Schuhmann, Romain Beaumont, Richard Vencu, Cade Gordon, Ross Wightman, Mehdi Cherti, Theo Coombes, Aarush Katta, Clayton Mullis, Mitchell Wortsman, Patrick Schramowski, Srivatsa Kundurthy, Katherine Crowson, Ludwig Schmidt, Robert Kaczmarczyk, and Jenia Jitsev. Laion-5b: an open large-scale dataset for training next generation image-text models. In *Adv. Neural Inform. Process. Syst.*, 2022. 6

[39] Pourya Shamsolmoali, Masoumeh Zareapoor, Huiyu Zhou, Michael Felsberg, Dacheng Tao, and Xuelong Li. From missing pieces to masterpieces: Image completion with context-adaptive diffusion. *IEEE Trans. Pattern Anal. Mach. Intell.*, 2025. 3

[40] Jiaming Song, Chenlin Meng, and Stefano Ermon. Denoising diffusion implicit models. In *Int. Conf. Learn. Represent.*, 2021. 1, 3

[41] Roman Suvorov, Elizaveta Logacheva, Anton Mashikhin, Anastasia Remizova, Arsenii Ashukha, Aleksei Silvestrov, Naejin Kong, Harshith Goka, Kiwoong Park, and Victor Lempitsky. Resolution-robust large mask inpainting with fourier convolutions. In *IEEE Winter Conf. Appl. Comput. Vis.*, 2022. 3

[42] Patrick von Platen, Suraj Patil, Anton Lozhkov, Pedro Cuenca, Nathan Lambert, Kashif Rasul, Mishig Davaadorj, Dhruv Nair, Sayak Paul, William Berman, Yiyi Xu, Steven Liu, and Thomas Wolf. Diffusers: State-of-the-art diffusion models. <https://github.com/huggingface/diffusers>, 2022. 6

[43] Qingsong Wang, Zhengchao Wan, Mikhail Belkin, and Yusu Wang. Seeds of structure: Patch pca reveals universal compositional cues in diffusion models. In *Adv. Neural Inform. Process. Syst.*, 2025. 2, 3

[44] Yinhui Wang, Jiwen Yu, and Jian Zhang. Zero-shot image restoration using denoising diffusion null-space model. In *Int. Conf. Learn. Represent.*, 2023. 3

[45] Yikai Wang, Chenjie Cao, Junqiu Yu, Ke Fan, Xiangyang Xue, and Yanwei Fu. Towards enhanced image inpainting: Mitigating unwanted object insertion and preserving color consistency. In *IEEE Conf. Comput. Vis. Pattern Recog.*, 2025. 3

[46] Zhou Wang, Alan Bovik, Hamid Sheikh, and Eero Simoncelli. Image quality assessment: From error visibility to structural similarity. *IEEE Trans. Image Process.*, 13, 2004. 2, 6

[47] Xiaoshi Wu, Yiming Hao, Keqiang Sun, Yixiong Chen, Feng Zhu, Rui Zhao, and Hongsheng Li. Human preference score v2: A solid benchmark for evaluating human preferences of text-to-image synthesis. *arXiv*, 2023. 2, 6

[48] Liangbin Xie, Daniil Pakhomov, Zhonghao Wang, Zongze Wu, Ziyan Chen, Yuqian Zhou, Haitian Zheng, Zhifei Zhang, Zhe Lin, Jiantao Zhou, and Chao Dong. Turbofill: Adapting few-step text-to-image model for fast image inpainting. In *IEEE Conf. Comput. Vis. Pattern Recog.*, 2025. 3

[49] Shaoan Xie, Zhifei Zhang, Zhe Lin, Tobias Hinz, and Kun Zhang. Smartbrush: Text and shape guided object inpainting with diffusion model. In *IEEE Conf. Comput. Vis. Pattern Recog.*, 2022. 3

[50] Jiazheng Xu, Xiao Liu, Yuchen Wu, Yuxuan Tong, Qinkai Li, Ming Ding, Jie Tang, and Yuxiao Dong. Imagereward: Learning and evaluating human preferences for text-to-image generation. In *Adv. Neural Inform. Process. Syst.*, 2023. 6

[51] Binxin Yang, Shuyang Gu, Bo Zhang, Ting Zhang, Xuejin Chen, Xiaoyan Sun, Dong Chen, and Fang Wen. Paint by example: Exemplar-based image editing with diffusion models. In *IEEE Conf. Comput. Vis. Pattern Recog.*, 2023. 3

[52] Shiyuan Yang, Xiaodong Chen, and Jing Liao. Uni-paint: A unified framework for multimodal image inpainting with pretrained diffusion model. In *ACM Int. Conf. Multimedia*, 2023. 3

[53] Jiwen Yu, Yinhui Wang, Chen Zhao, Bernard Ghanem, and Jian Zhang. Freedom: Training-free energy-guided conditional diffusion model. In *Int. Conf. Comput. Vis.*, 2023. 2, 4

[54] Guanhua Zhang, Jiabao Ji, Yang Zhang, Mo Yu, Tommi Jaakkola, and Shiyu Chang. Towards coherent image in-

painting using denoising diffusion implicit models. In *International Conference on Machine Learning*, 2023. 3

[55] Lvmin Zhang, Anyi Rao, and Maneesh Agrawala. Adding conditional control to text-to-image diffusion models. In *Int. Conf. Comput. Vis.*, 2023. 2

[56] Richard Zhang, Phillip Isola, Alexei A Efros, Eli Shechtman, and Oliver Wang. The unreasonable effectiveness of deep features as a perceptual metric. In *IEEE Conf. Comput. Vis. Pattern Recog.*, 2018. 2, 6

[57] Junhao Zhuang, Yanhong Zeng, Wenran Liu, Chun Yuan, and Kai Chen. A task is worth one word: Learning with task prompts for high-quality versatile image inpainting. In *Eur. Conf. Comput. Vis.*, 2024. 1, 3

5.1. Prompt for example figures

The following prompt was used for Figs. 2, 3, 5 and 6.

A high quality, 4K, realistic image of bright red mushrooms with white speckles growing in a cluster at the base of a smooth gray tree trunk. Fallen orange and brown autumn leaves cover the ground with patches of green grass and a couple of round gray stones nearby. Yellow-green leaves hang above.

5.2. Exact prompt for generating prompts

Given the masked image directories, we instruct Claude [4] to generate image prompts using the following templates. Variables denoted in **blue** are populated programmatically in a loop.

FFHQ

Manually generate caption ID **[INDEX]** of the folder **[Masked Image Folder]** and output each caption to **[Output Text File Path]** as **caption_[INDEX].txt**. Process one image at a time (not in batches) and overwrite existing files. Each caption must be 2--3 concise sentences that describe the complete, fully restored scene as it should look after inpainting. Use the visible context to infer plausible colors, materials, geometry, and lighting; extend existing structures smoothly and remain consistent with the overall style of the source image. In the final prompt that you output, definitely remove any descriptions related to "mask" or "grey area". We want a prompt that describes the final inpainted image without the mask. Also, remove anything about symmetrical in the caption. Be succinct, using only a few sentences. Directly use your write operation. Do not do any bash commands such as cat and >>.

DIV2K

Manually generate one caption per PNG inside **[Masked Image Folder]**, processing the images sequentially and never batching. Reference the mask layout encoded in **[Mask Tensor Path]** so you can infer what content should appear in the hidden region, but do not mention the mask itself in the final writing. For each image, write the caption directly (no shell redirection) to **[Output Caption**

Folder] /caption_**[image_INDEX]**.txt (e.g., caption_00039.txt). Each caption must be 2--3 tight sentences that describe the complete, fully restored scene as it should look after inpainting. Use the visible context to infer plausible colors, materials, geometry, and lighting; extend existing structures smoothly and stay consistent with the overall style of the source image. Do not introduce new objects, camera moves, or artistic flourishes that are not already implied. Absolutely avoid words such as "mask," "grey area," "missing," "occluded," or any hint that parts of the image were blocked out---the caption should read like a finished description of the final inpainted result only.

5.3. Additional Qualitatives

The figures below show randomly selected samples of inpainted results for all baselines and our method. Zoom in for better detail.



Figure 8. Qualitative comparison of inpainting results on FFHQ dataset. 15 samples drawn at random from the full set of 1000 outputs.



Figure 9. Qualitative comparison of inpainting results on DIV2K dataset. 15 samples drawn at random from the full set of 800 outputs.

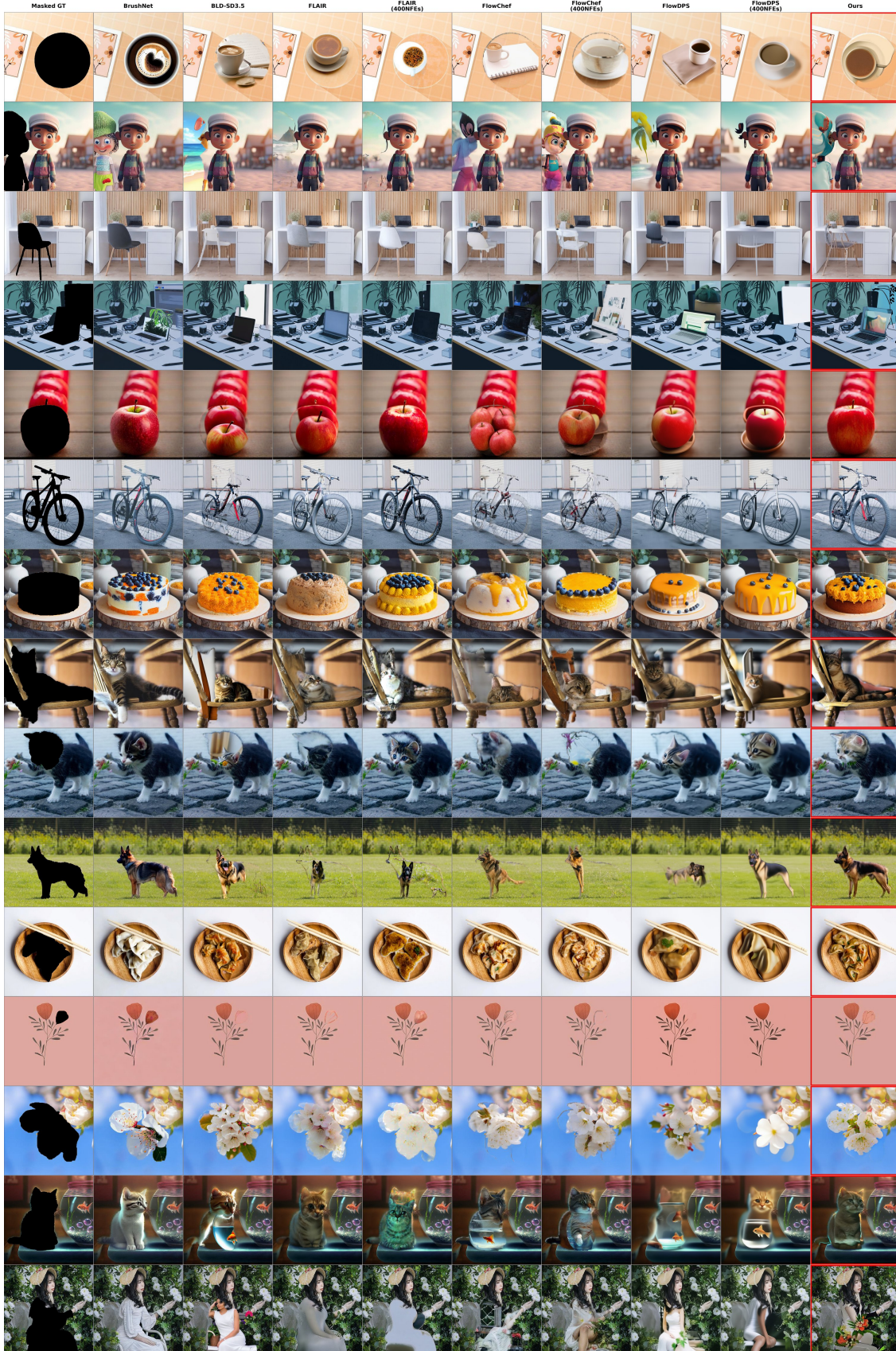


Figure 10. Qualitative comparison of inpainting results on BrushBench dataset. 15 samples drawn at random from the full set of 600 outputs.